Applied Ocean Research
September 2023, Volume 138 Pages 103626 (11p.)
https://doi.org/10.1016/j.apor.2023.103626
https://archimer.ifremer.fr/doc/00842/95399/

Misaligned sheared flow effects on a ducted twin vertical axis tidal turbine

Moreau Martin [1, *], Germain Gregory [1], Maurice Guillaume [2]

[1] Ifremer, Marine Hydrodynamics Laboratory, 150 Quai Gambetta, Boulogne-sur-mer, 62200, France
[2] HydroQuest SAS, 16 Chemin de Malacher, Meylan, 38240, France

* Corresponding author : Martin Moreau, email address : mmoreau@ifremer.fr

ggermain@ifremer.fr ; guillaume.maurice@hydroquest.net

Abstract :

Most tidal turbines experimental tests are carried out in idealised conditions with uniform velocity profiles and without flow misalignment. However, at sea, the velocity profiles are mostly sheared and the flow direction spreads out around the main direction. In this study, we address experimentally the effect of those realistic conditions on the response of a twin counter-rotating vertical axis tidal turbine in Ifremer's wave and current flume tank. At the whole turbine scale, the current shear hardly affects the drag and the average power coefficient but it leads to a 35 % increase of the power standard deviation. The flow misalignment does not affect the power production but it raises the average drag coefficient by 15 % for a ±15°angle of incidence. At the rotor column scale, both the shear and the misalignment modify the torque distribution with regard to the blades angular position, with a torque asymmetry up to 30 % between the upper and lower rotors, among other effects. Absolute rotor angular position as well as blades local flow visualisation would be needed to explain the complex torque distribution on a rotor column, which must be taken into account in the turbine design. This paper also provides a wide experimental database for the validation of numerical models applied to ducted twin vertical axis tidal turbines.

Highlights

► Tidal currents are vertically sheared with variable directions in time and space. ► Tank testing of a 1/20 scale twin vertical axis turbine (2-VATT) in sheared flow. ► 2-VATT in flood and ebb tide configurations with 5 relative angles of incidence. ► The average power coefficient is unaffected by the flow shear and misalignment. ► Sheared flows extend the torque and power fluctuations of the 2-VATT.

Keywords : Tidal energy, Vertical axis turbine, Tank experiment, Sheared current, Flow misalignment

1. Introduction

At sea, tidal turbines are subject to complex current conditions depending on the site considered. Many studies on different locations identified for their high tidal currents reveal the presence of waves, turbulent flows, sheared velocity profiles and flow direction variability [2, 7, 12, 26, 15]. For instance, at Paimpol-Bréhat test site, France, the turbulent intensity is evaluated about 15 % [5] and extreme wave conditions up to 6 m significant wave height with 12 s peak period were observed between 2019 and 2021 [23]. In addition, the vertical velocity profile is sheared with about 20 % velocity difference between the top and the bottom of the turbine capture area, and the average direction asymmetry between ebb and flood tides at this location is about 22° (Fig. 1).

Before testing full-scale devices at sea, tidal turbines are first studied numerically and at reduced-scale in flume or towing tanks [9, 11, 16]. Apart from the dynamic loads induced by turbulence [4, 29] and waves [3, 18], the effects of both sheared and misaligned incident flow have not been addressed thoroughly yet. A few studies considered Horizontal Axis Tidal Turbines (HATT) in collinear sheared flow [1, 17, 31]. Overall, they reveal an increase of about 30 % in torque and about 50 % in thrust fluctuations due to the flow asymmetry between the upper and lower part of the rotor disc. Furthermore, other studies analysed the effect of flow misalignment on HATT with uniform velocity profiles [6, 21]. They reveal a power reduction of 7 % and 9 % for a flow misalignment of 10° and 15°, respectively, by numerical and experimental approaches. The addition of a shroud around a HATT induces a reduction of the misalignment effect as only about 6 % of power loss were obtained for a shrouded turbine against 23 % for the free turbine with 25° misalignment [27].

Beside HATT, Vertical Axis Tidal Turbines (VATT) are also good candidates for tidal energy harvesting due to their performance insensitivity to the flow direction among other advantages [25, 19], but those turbines have been less studied until now. Only a few studies considered single vertical axis wind turbines facing vertically sheared velocity profiles [28]. Mendoza et al. [19] studied the performance and wake of such a wind turbine under varying surface roughness conditions, generating varying vertical shear and turbulence levels. They found minor influence of these

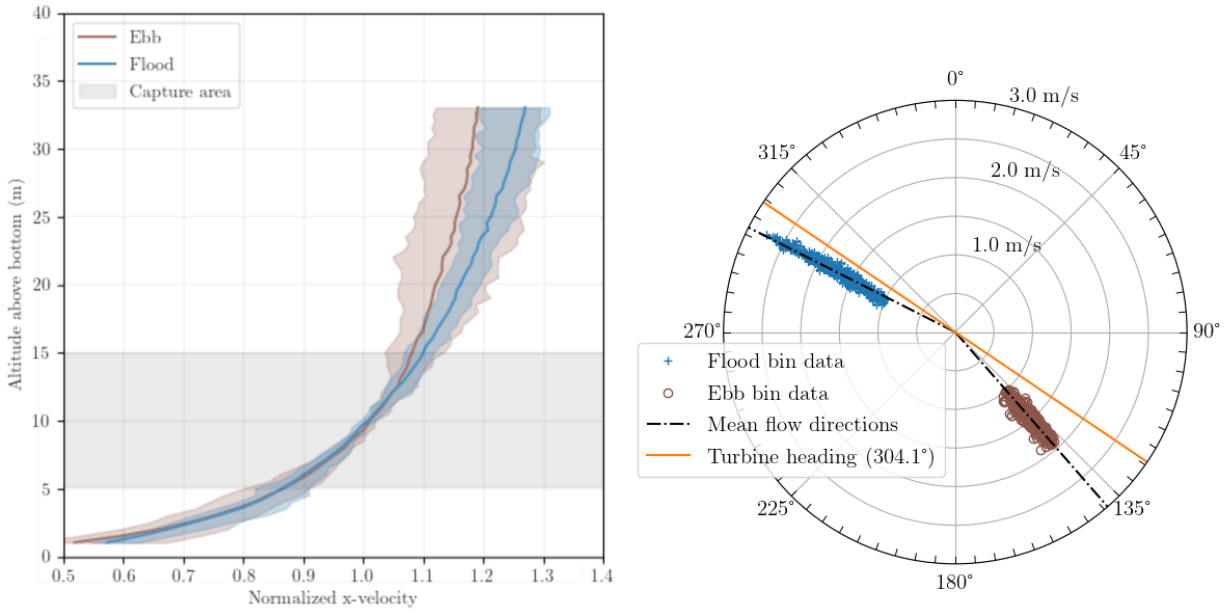

Figure 1: Paimpol-Bréhat test site flow characteristics [23]: (left) Vertical average velocity profiles during flood and ebb tides. The solid lines stand for the mean profiles and the shades for the range between minimal and maximal values. (right) Tidal current magnitudes and origin directions at the height of *HydroQuest*'s tidal turbine demonstrator centre.

conditions on the power coefficient and a faster wake recovery with the most sheared and turbulent velocity profile, rather explained by the turbulence mixing improvement than the vertical shear.

Furthermore, it was found that placing two counter-rotating vertical axis turbines side by side improves the power performance significantly and reduces the vertical torque on the turbine base [14, 30]. Taking advantage of those results, *HydroQuest* develops Twin Vertical Axis Tidal Turbines (2-VATT) and tested a 1 MW-rated ducted device at Paimpol-Bréhat offshore test site [10, 23]. The performance and the wake of that device was studied at a $1/20^{\text{th}}$ scale in a tank in idealised current conditions (uniform velocity profile with collinear ebb and flood directions) [22]. The results showed a difference of optimal tip speed ratio and of power fluctuation between ebb and flood tide orientations whereas the maximal average power and drag coefficients were hardly affected. However, to the authors knowledge, the effect on twin vertical axis tidal or wind turbines of the incident flow shear or its relative misalignment with the turbine heading has never been studied.

In the present work, the effect on the above mentioned reduced-scale ducted 2-VATT of both the flow shear and its misalignment is analysed based on experiments in Ifremer's wave and current flume tank (Fig. 2). The section 2 presents the turbine model and its setup in the tank (2.1) before describing the data acquisition and processing methods (2.2). Next, the section 3 presents the effect of the shear in aligned flow conditions (3.1) and the effect of the flow misalignment with a sheared flow (3.2) on the behaviour of the ducted 2-VATT. Finally, the results are discussed with the help of upstream flow measurements in the section 4.

2. Material and method

2.1. Experimental setup

The 2-VATT 1/20 scale model is geometrically similar to the full-scale 1 MW-rated demonstrator tested by *HydroQuest* at Paimpol-Bréhat test site [24]. It is composed of two independent counter-rotating vertical axis rotor columns. Each column is made of two levels of rotors with a 60° phase difference between them, and each rotor of radius $R = D/2 = 200$ mm is made of $N = 3$ blades with a height (H_{blade}) of 190 mm and a chord (c) of 73 mm. Thus, the rotors solidity (Nc/R) is 1.1, similarly to the full-scale demonstrator. The rotors are mounted in a structure made of fairings and plates. The turbine height is defined as the distance between the top and the bottom horizontal plates such that $H = 450$ mm. The turbine is fixed on a bottom-mounted base, either a tripod similar to the demonstrator's base or

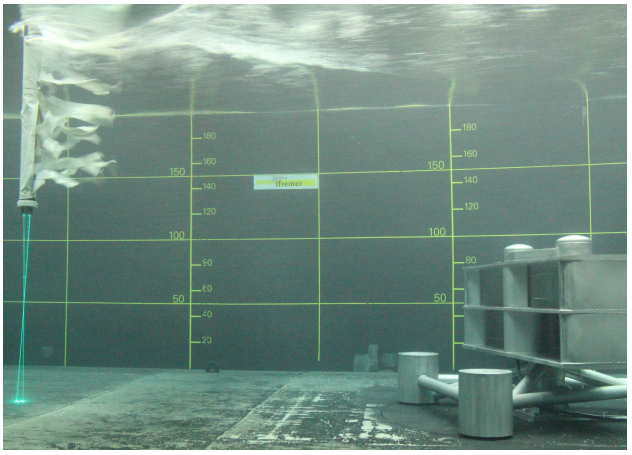

Figure 2: 2C-LDV measurement in the Ifremer's tank upstream of the ducted 2-VATT model in ebb tide configuration with $-15°$ misalignment between the flow direction and the turbine heading.

Table 1
Recap of the main similitude values between tank tests and in-situ operation at Paimpol-Bréhat, with $g = 9.81$ m.s^{-2} the gravity constant, $\nu = 1.05\ 10^{-6}$ m^2.s^{-1} the water kinematic viscosity and $\lambda = 1.5$ the tip speed ratio (Eq. 4).

Scale	Water depth H_{wat} (m)	Structure height H_{struc} (m)	Flow velocity U (m.s^{-1})	Froude number $Fr_s = \frac{U}{\sqrt{g(H_{wat}-H_{struc})}}$	Reynolds number $Re_c = \frac{\lambda c U}{\nu}$
1/20	2	0.84	1.0	0.30	$1.0\ 10^5$
1/1	40	17	2.5	0.17	$5.2\ 10^6$

a central monopile of the same height. The results presented in this study are with the tripod base. The 2-VATT model is tested in Ifremer's 2 m deep and 4 m wide wave and current flume tank in Boulogne-sur-mer, France, at a velocity set point of 1 m.s^{-1} (Fig. 2) [8]. The orthogonal coordinates system considered is such that x is in the current direction with its origin at the centre of the model and z points towards the surface with its origin at the bottom plate of the turbine, such that the turbine capture height ranges between $z/H = 0$ and 1. The model, its instrumentation and the setup in the tank are fully described in Moreau et al. [22]. The main similitude quantities between reduced- and full-scale are presented in Tab. 1. The Reynolds number at full-scale is about 50 times higher than in the present experiment, which is expected to reduce the blades performance [20]. The Froude number based on the turbine submergence (Tab. 1) is 1.8 times higher in the tank than at sea but it remains low enough to avoid interactions with the free surface.

To generate low turbulence flows in the tank, the inlet is conditioned by a grid and a honeycomb structure (Fig. 3 (a)). Usually, the grid is homogeneous over the tank section and provides a uniform velocity profile with a $0.6H$ high boundary layer (Fig. 4). To generate a sheared current similar to what was measured at Paimpol-Bréhat test site, we developed a special apparatus presented in [17, 24]. The latter consists of a panel made of multiple layers of wire meshes fixed on the grid upstream of the honeycomb (Fig. 3 (b)). The multiple layers are non-uniformly distributed along the vertical direction and are uniform along the tank width. Thus, the panel generates variable friction losses along the height leading to a vertically sheared current profile downstream on the whole tank width. The streamwise average velocity and turbulence intensity profiles at the turbine position in the empty tank are presented in Fig. 4. The streamwise turbulence intensity is defined as $TI_u = \sigma(u)/\overline{u}$, with u the streamwise velocity, the bar on top indicating the time average and $\sigma(\ )$ the time standard deviation of the quantity between brackets. The sheared average velocity profile power law fit is consistent with such fits at sea [2, 15, 24] and provides a 13 % velocity difference between the top and the bottom of the turbine capture area.

Furthermore, the flow angle of incidence (α) with regard to the 2-VATT heading was of -7° at flood tides and +15° at ebb tides during full-scale demonstration [23]. In the present paper, we also study the effect of those flow misalignments on the turbine behaviour in presence of the sheared velocity profile in the tank. The model 2-VATT is set in the two flow directions representing Flood and Ebb tide Configurations (FC and EC respectively) at Paimpol-Bréhat test site.

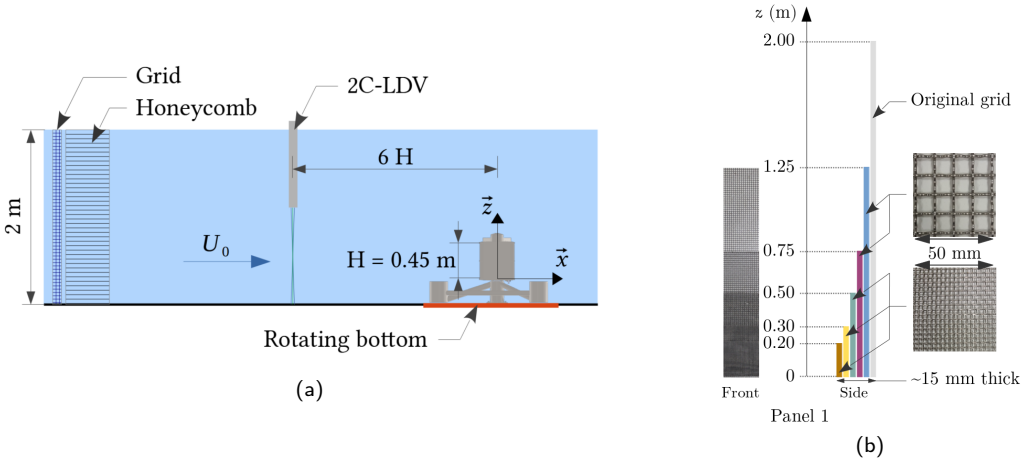

Figure 3: (a) Scheme of the experimental setup in the Ifremer's wave and current flume tank. (b) Scheme of the grid arrangement developed for the generation of a sheared velocity profile, with $z = 0$ m at the tank bottom.

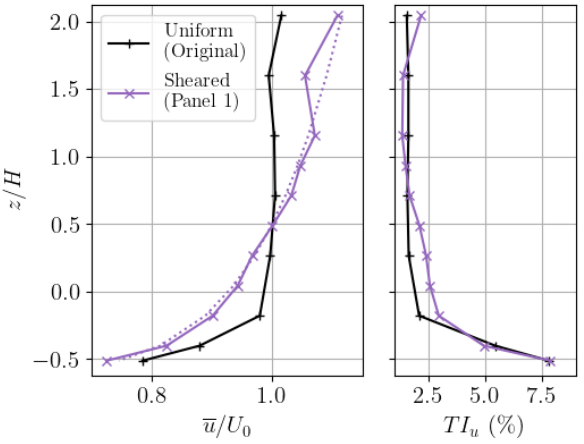

Figure 4: Mean normalised streamwise velocity and turbulence intensity profiles measured with the 3C-LDV probe at the center of the tank without turbine, with $z/H = 0$ at the turbine bottom. The sheared average velocity profile fit (purple point line) is $\overline{u}/U_0 = \left(\frac{z/H}{0.24H_w}\right)^{1/7.91}$.

For each configuration, we test five relative angles of incidence: 0°, ± 7° and ± 15° (Fig. 5). To do so, the model is fixed either in FC or EC on the rotating bottom of the tank. Then, it is rotated using the automated rotating system from -15° to +15° (Fig. 3 (a)).

2.2. Data acquisition and processing

For hydrodynamic performance assessment, the current velocity is measured using a *Dantec* 2-Component Laser Doppler Velocimeter (2C-LDV). The latter measures the velocity along (x, y) in non-coincident mode with an acquisition data rate of the order of 200 Hz. The probe is placed at $x/H = -6$, at the centre of the turbine projected area (ie. $(y, z) = (0, 0.5)H$). At this point, the average u and v are undisturbed by the TEC induction and remain the same whatever the turbine configuration and misalignment. The average streamwise component of the velocity at this point, which is equal to the average over the turbine height for the two velocity profiles, is considered as the reference velocity (noted U_0) and is 0.945±0.005 m.s^{-1} overall. Synchronously with the 2C-LDV, each rotor column torque (Q), rotational speed (ω) and the 6 load components applied between the turbine and the base are acquired using *National*

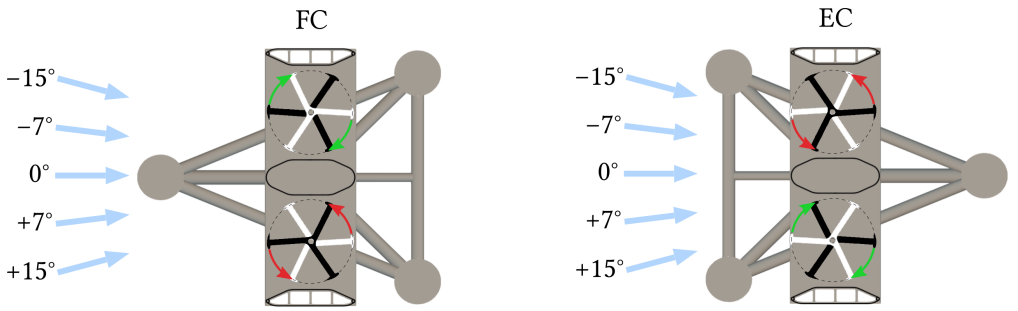

Figure 5: Schematic top view of the ducted 2-VATT with the flow angles of incidence tested in the tank both in the Flood and Ebb tide Configurations (FC and EC respectively).

Instruments PXI and *LabView* systems. The acquisitions last 3 minutes with a 128 Hz sampling frequency to guarantee the time convergence of the mean and standard deviation of the signals.

The power extracted by the 2-VATT is analysed at two scales. At the rotor column scale, we compute the instantaneous power $P_{col}(t) = Q(t)\omega(t)$ with t the time. The torque signal considered $Q(t)$ considered is the measured value corrected by the friction torque due to the seals and the transmission system between the rotors and the torque meter [22]. The column power coefficient (C_{Pcol}, Eq. 1 with $\rho = 1000\,\mathrm{kg.m^{-3}}$) is computed with the two rotors projected area as a reference surface ($S = 2DH_{blade}$). At the turbine scale, we also compute the instantaneous total power (P) as the sum of the power extracted by the two rotor columns. The turbine power coefficient (C_P, Eq. 2) is computed with the four rotors projected area as the reference surface ($S = 4DH_{blade}$). The fluctuation of this quantity depends on the random relative phase between the two columns. By nature, VATT loads fluctuate periodically at the blade passing frequency. If the two columns are in phase, the sum of their instantaneous power doubles the periodical fluctuation, similarly to constructive interferences, assuming a perfect symmetry between the two columns. Conversely, if they are in perfect phase opposition, these fluctuations vanish, similarly to destructive interferences. Thus, given the randomness of those interferences, the standard deviation of the instantaneous total power is irrelevant to study the physical effect of flow condition changes on the behaviour of the 2-VATT. Instead, we define $\overline{\sigma}(C_{Pcol})$ as the average of the standard deviation of the two columns power coefficients to better represent the mechanical fluctuations perceived by the whole turbine.

$$C_{Pcol}(t) = \frac{P_{col}(t)}{\rho D H_{blade} U_0^3} \tag{1}$$

$$C_P(t) = \frac{P(t)}{2\rho D H_{blade} U_0^3} \tag{2}$$

In addition, the drag coefficient is computed using F_x, the load in the streamwise direction measured between the turbine and the base, considering the projected area of the four rotors as the reference surface (Eq. 3). The power and drag results are presented with regard to the tip speed ratio (λ) defined in Eq. 4. The distribution of the torque coefficient (C_Q, Eq. 5) along the rotor angular position of the green column (Fig. 5) is also analysed. The instantaneous relative angular position (positive in the rotation direction) is computed by Hilbert transform of the torque signal filtered around the rotational frequency. The angular position being relative, the absolute angle values displayed cannot be compared between graphs. The phase average, indicated by a tilde on top of the symbol, is computed over 75 revolutions with 3° angle bins. The phase shift between torque maxima are computed by identifying the locations of the smoothed torque phase average maxima. The smoothing is obtained by a low-pass third order Butterworth filter.

$$C_x(t) = \frac{F_x(t)}{2\rho D H_{blade} U_0^2} \tag{3}$$

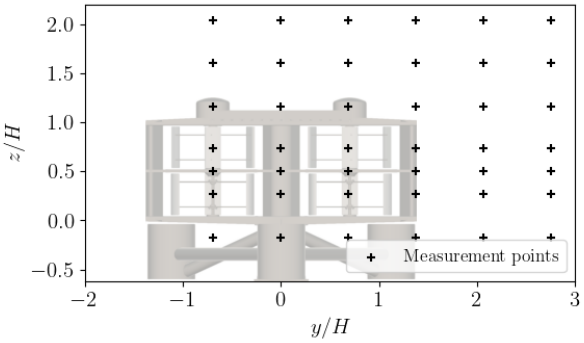

Figure 6: Points mesh used for velocity measurements with the 3C-LDV at $x/H = 3$.

$$\lambda(t) = \frac{\omega(t)R}{U_0} \tag{4}$$

$$C_Q(t) = \frac{Q(t)}{\rho D H_{blade} R U_0^2} \tag{5}$$

Furthermore, the flow surrounding the ducted 2-VATT is characterised at $\lambda = 1.6$ in FC and EC for the uniform and the sheared velocity profiles without flow misalignments. The measurements are conducted with a *Dantec* 3-Component LDV, in non-coincident mode, as described in [22]. The velocity maps presented hereinafter are drawn based on linear interpolations between the mesh points (Fig. 6) with a 40 mm step in the y and z directions.

3. Flow shear and misalignment effects

First, we analyse the effect of a sheared incident flow compared to a uniform one, collinear with the turbine heading. Then, the impact of flow misalignments added to the shear is presented. In the two sections, we study the overall performance of the 2-VATT in terms of power and drag before addressing the effect at a single rotor column scale.

3.1. Aligned sheared flow effect

Fig. 7 displays the drag and power coefficients of the turbine facing the uniform and the sheared flows both in EC and FC. The results show that the ducted 2-VATT drag is insensitive to the incident velocity profile, both in terms of average and standard deviation. We only observe differences of $\sigma(Cx)$ at $\lambda = 1.9$ that are related to vibrations of the model. The average power coefficient is also hardly affected by the flow shear given the measurements repeatability (Fig. 7 (b)). However, the power fluctuations strongly increase with the sheared flow as the standard deviation rises by 35 % at the optimal operating point (λ_{opt}, where $\overline{C_P}$ is maximal), both in EC and FC.

To look at the shear effect at the rotors scale, Fig. 8 displays the torque coefficient with regard to a relative angular position at λ_{opt} facing the uniform flow (a & c) and the sheared flow (b & d) in EC and FC. On one hand, in uniform flow, the distribution in FC is more smoothed than in EC where the torque peaks and troughs are more pronounced. We also observe about 20 % difference between the torque generated by the two levels of rotors in EC while the contribution of the two levels is rather balanced in FC. The phase averaged torque maxima are separated by 60° in EC, similarly to the geometrical phase difference between the upper and the lower rotors. However, we observe an additional phase shift $\Phi_Q = 5°$ compared to the geometrical phase between the torque peaks of the upper and the lower rotors in FC. The differences between EC and FC in uniform flow are discussed in depth in Moreau et al. [22] and are due both to the tripod base asymmetry and to the difference of counter-rotation direction. On the other hand, when the turbine is placed in a sheared flow, a strong torque asymmetry appears between the two rotor levels as three of the peaks are about 30 % lower than the three others, both in FC and EC. In addition, a significant additional phase shift $\Phi_Q = 9°$ appears between the torque peaks of the top and the bottom rotors for the two configurations.

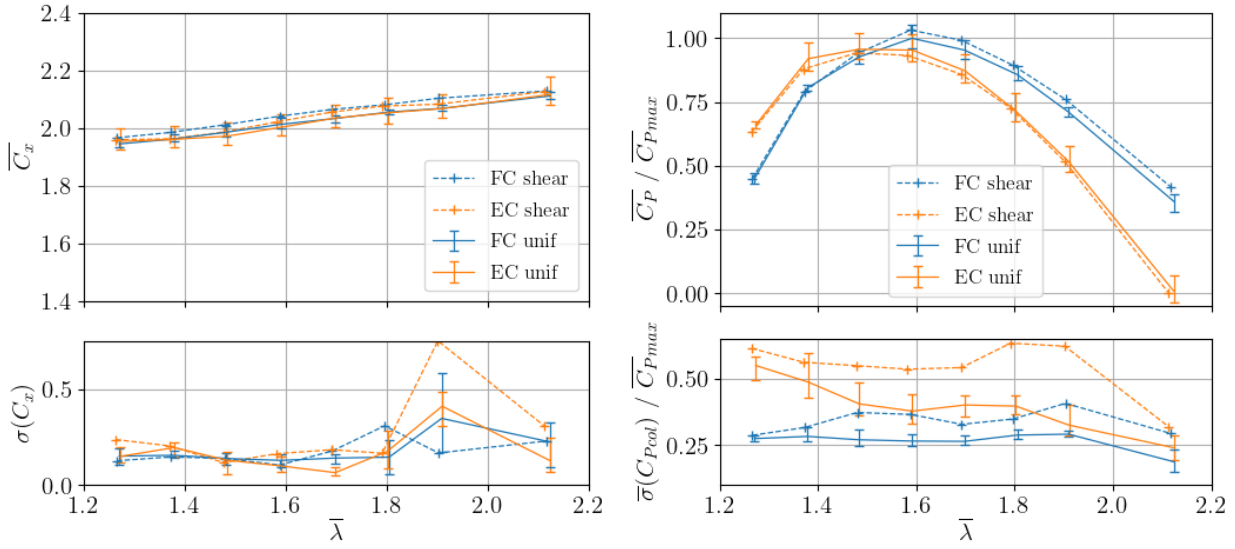

(a) Drag coefficient (b) Power coefficient

Figure 7: Average (top) and standard deviation (bottom) of the drag and power coefficients in FC and EC with sheared and uniform incident velocity profiles. The curves with the uniform velocity profile are averages over 3 test campaigns with the error bars representing the extreme average and extreme standard deviation values over the 3 campaigns. The C_P are normalised by the maximal average value in "FC unif".

The Fourier Transform of the torque (Q) presented in Fig. 9 reveals the effect of the flow shear on the frequency content of the green column torque in FC. The results show that the component at 6 times the rotational frequency (f_ω), representing the 6 blades that compose the column, is dominant both in the uniform and the sheared flows. However, the amplitude ratio between the peaks at $3f_\omega$ and $6f_\omega$ is more than doubled in the sheared flow compared to the uniform flow, which is congruent with the phase shift and amplitude asymmetry observed in the torque angular distributions. This result is observed in EC as well as in FC although not plotted here.

Beyond the turbine performance, Fig. 10 displays the average streamwise velocity in the wake of the ducted 2-VATT facing the uniform flow in FC and EC (a & c) and facing the sheared flow (b & d). In the four cases, the turbine operates at $\lambda = 1.6$ and the measurements are at $x/H = 3$. Apart from the incident shear that is also identified downstream of the turbine, the wake geometry seems unchanged. Indeed, as it is described in Moreau et al. [22], at this downstream position, the wake of the two columns are merged in FC but not in EC, regardless of the incident velocity profile. The dynamics in (v, w) is also barely affected by the shear with large swirls around the x axis in FC that are less present in EC.

3.2. Misaligned sheared flow effect

To go further in the reproduction of realistic tidal current conditions in the tank experiments, we add flow misalignment to the sheared velocity profile. Fig. 11 displays average and standard deviation of the drag and power coefficients of the ducted 2-VATT in the flood tide configuration with five flow angles of incidence (α) between $-15°$ and $+15°$. On one hand, it appears that $\overline{Cx}$ increases with α up to 15 % when $\alpha = \pm 15°$ compared to the case at $\alpha = 0°$. That evolution is symmetrical in the positive and negative angles of incidence but it is not linear with the angle. We observe no effect on the drag fluctuations though. On the other hand, the flow misalignment with the turbine heading hardly affects the power coefficient both in terms of average and fluctuation. The same observations can be made on the performance at the whole turbine scale when studying the turbine in EC as well as on the monopile base (not plotted).

However, when we look at the rotor column scale, the misalignment affects significantly the power extraction. Fig. 12 displays the power coefficient of the green rotor column with regard to the tip speed ratio in FC and EC. At first glance, we observe that the average power coefficient increases when α increases in the negative side and that it slightly decreases with a widening of the curve when α increases in the positive side. When $\alpha < 0$, that green rotor column is

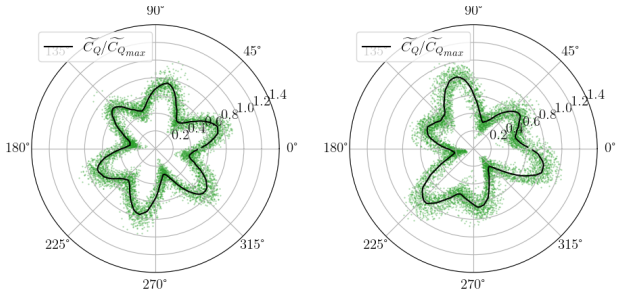

(a) FC in uniform flow (b) FC in sheared flow

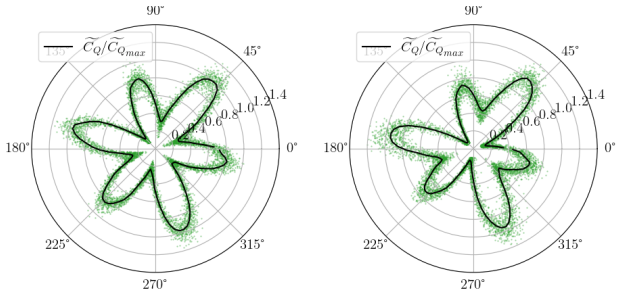

(c) EC in uniform flow (d) EC in sheared flow

Figure 8: Angular distribution of the green rotor column torque coefficient for the two aligned flow directions and the two velocity profiles at the optimal λ (1.6 in FC and 1.5 in EC). The green dots are the instantaneous measurements and the black line is the phase average. The values are normalised by the maximal phase average value in EC in uniform flow. *Reminder*: the angular position is relative, so the absolute angle values cannot be compared between graphs.

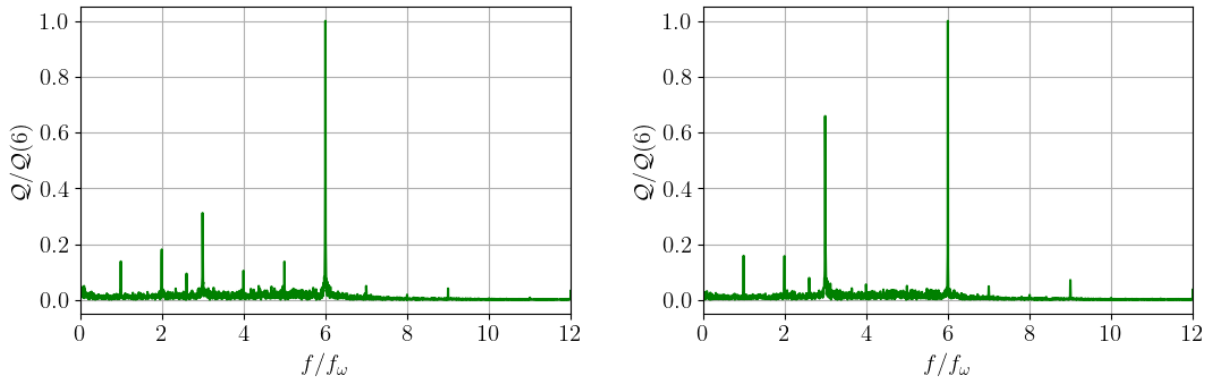

(a) FC in uniform flow (b) FC in sheared flow

Figure 9: Fourier transform of the green column torque in FC at the optimal operating point. The frequencies are normalised by the rotational frequency (f_ω) and the amplitudes by the one of the peak at $6f_\omega$.

downstream of the red column in EC while it is upstream in FC, and vice versa (Fig. 5). Thus, the tendency with regard to the angle is reversed between FC and EC: $\overline{C_{Pcol}}$ increases when the rotor column goes upstream in FC whereas that increase occurs when the column is downstream in EC. Note that those tendencies are the same with the 2-VATT fixed on the monopile base so they are not due to the base asymmetry. Furthermore, we notice that the flow misalignment

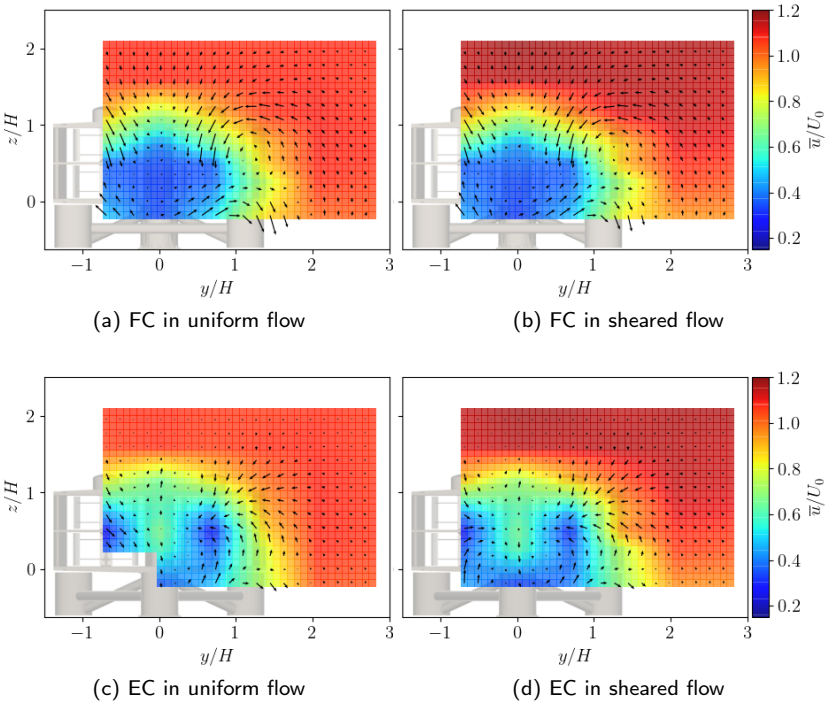

(a) FC in uniform flow (b) FC in sheared flow

(c) EC in uniform flow (d) EC in sheared flow

Figure 10: Maps of the mean streamwise velocity ($\overline{u}/U_0$) in (y,z) planes at $x/H = 3$, viewed from downstream, with superimposition of an arrow field representing the mean transverse velocities $(\overline{v},\overline{w})/U_0$.

induces an increase of the standard deviation of the column power coefficient in EC from $\alpha = -15$ to $+15°$, mainly at low λ, whereas no trend appears in FC.

The torque angular distribution evolution with the angle of incidence shows that the evolution of C_{Pcol} relies on different physical phenomena between FC and EC (Fig. 13). In EC, the torque distribution is rather unchanged by α. Only the overall torque magnitude increases when α decreases leading to the increase of $\overline{C_{Pcol}}$ when the column goes downstream. In FC, the torque angular distribution is modified by the angle of incidence as it affects the asymmetry between the upper and the lower rotors. When α goes negative, the phase difference between the upper and the lower rotors remains but the contribution of the two levels of rotors balances and increases the C_{Pcol}. Whereas, when α goes positive, the difference of torque amplitude due to the shear is unaffected but the phase difference between the two levels of rotors goes back closer to the geometrical phase. Those tendencies in FC intensify when α increases up to $\pm 15°$ and they are similar on the monopile base. Finally, despite those differences between FC and EC, the maximal $\widetilde{C_Q}$ appears when the column is downstream of the other rotor column in the two configurations (at $+15°$ in FC and -15° in EC).

Similarly, the relative contribution of the $3f_\omega$ and $6f_\omega$ harmonics in the torque Fourier transform evolves differently with α in EC and FC (Fig. 14). In FC, the peaks amplitude ratio decrease compared to the aligned configuration whether with positive or negative misalignments. Whereas in EC, the contribution of $3f_\omega$ tends to decrease with positive misalignment angles and increase with negative α.

4. Discussion

Section 3.1 revealed that the whole turbine drag and average power performance are unaffected by the incident current shear. However, we saw that the power standard deviation increases by 35 % at the optimal operating point which goes along with the modification of the torque angular distribution. Indeed, when the incident current is sheared, the torque peaks of one of the rotors (either the upper or the lower one of the column) are about 30 % higher than those of the other rotor and an additional phase shift of 9° compared to the geometrical phase between the blades appears between the two rotor levels. In the spectral analysis of the torque, the shear effect manifests through a 2 times higher

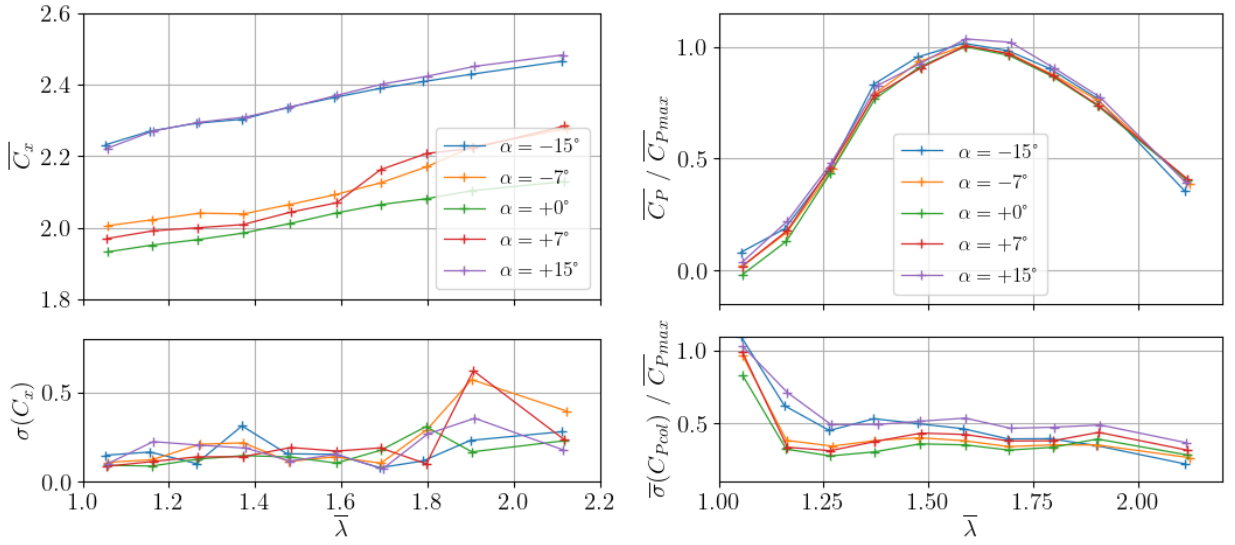

(a) Drag coefficient (b) Power coefficient

Figure 11: Average and standard deviation of the drag and power coefficients in FC with the sheared velocity profile and various misalignment angles. The power coefficients are normalised by the maximal $\overline{C_P}$ at $\alpha = 0°$.

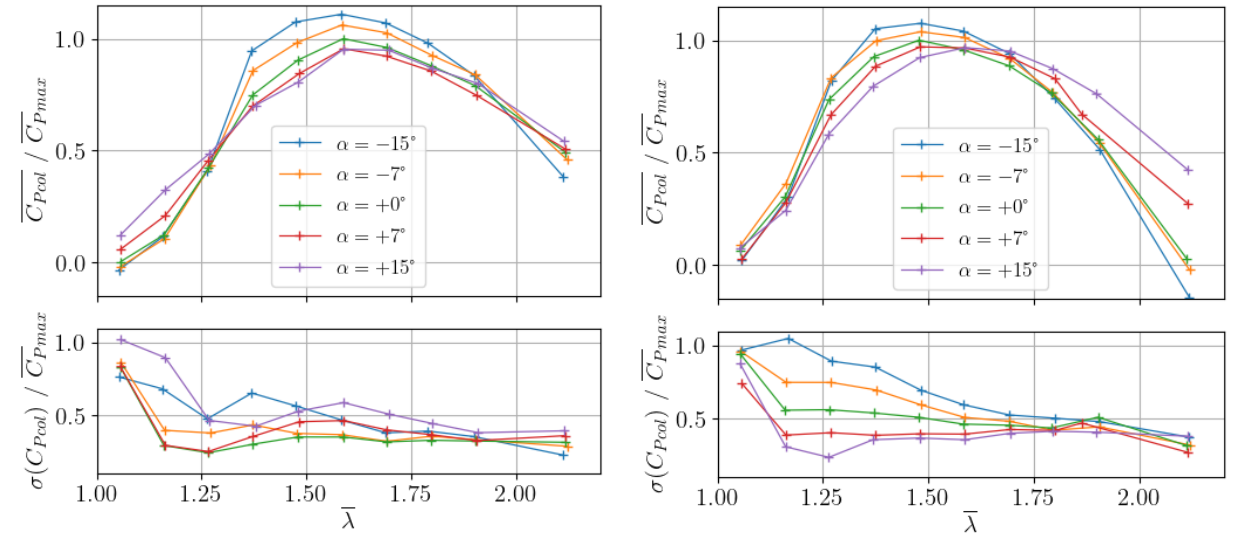

(a) Green column power coefficient in FC (b) Green column power coefficient in EC

Figure 12: Average and standard deviation of the green rotor column power coefficients in FC and EC with the sheared velocity profile and various misalignment angles, normalised by the maximal $\overline{C_{Pcol}}$ at $\alpha = 0°$ in each plot.

contribution of the peak at $3f_\omega$ relatively to that of the peak at $6f_\omega$ with the sheared flow compared to the uniform flow. Fig. 15 and 16 present profiles of the streamwise velocity at x/H = -1 in front of the turbine in EC with both the uniform and the sheared flow. In EC, the base feet are in front of the outer part of the bottom rotors and their bypassing affects the velocity perceived by the turbine [22]. With the uniform flow, the base bypassing generates an important velocity increase in front of the bottom rotors, so we assume that the bottom rotors recover more torque from the flow than the upper ones. Conversely, with the sheared flow, the base bypassing also generates a velocity increase in front of the bottom rotors but this only reduces the initial shear. As a consequence, the bottom rotors still perceive a lower

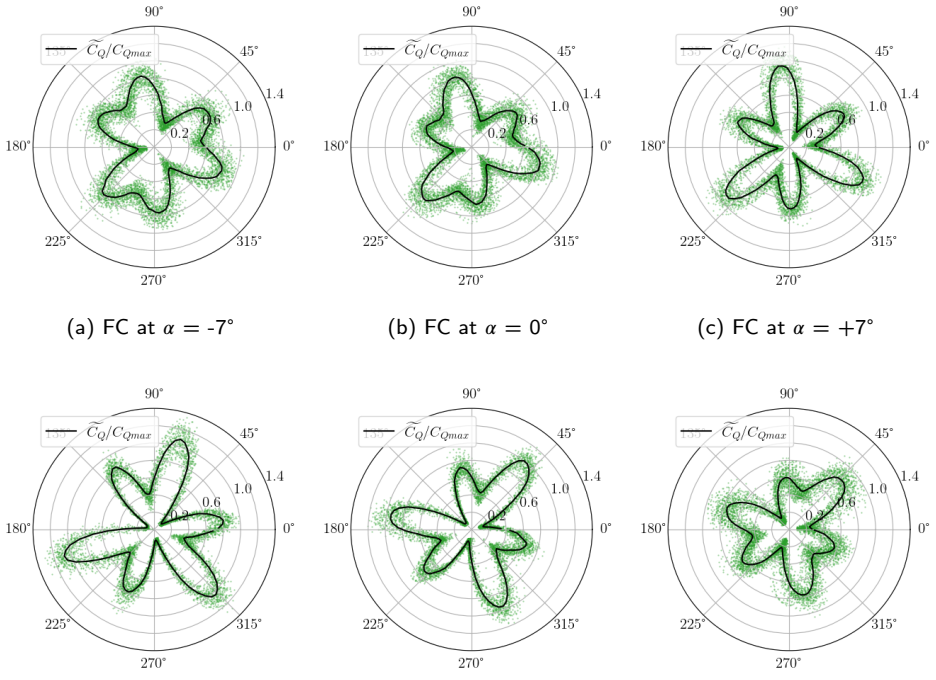

(a) FC at α = -7° (b) FC at α = 0° (c) FC at α = +7°

(d) EC at α = -7° (e) EC at α = 0° (f) EC at α = +7°

Figure 13: Angular distribution of the torque coefficient for the green rotor column for the two flow orientations at the optimal λ (1.6 in FC and 1.5 in EC) with the sheared velocity profile and various misalignment angles. Torques are normalised by the maximal phase average in EC at $\alpha = 0°$. The green dots are the instantaneous measurements and the black line is the phase average. *Reminder*: the angular position is relative, so the absolute angle values cannot be compared between graphs.

velocity than the top rotors. In FC, the single central base foot by-passing does not interact significantly with the flow in front of the rotors (not presented here). So we assume that, with a sheared incident current profile, the greatest torque peaks observed in Fig. 8 are generated by the upper rotor due to the higher flow velocity squared, both in FC and EC. In addition, since the upper and lower rotors are fixed together and kept at a constant rotational speed, the velocity asymmetry in the sheared current induces a difference of λ between the two rotor levels. For vertical axis turbines, the absolute angular position of maximal C_Q varies with λ [13]. Consequently, the phase between the upper and lower rotors torque peaks differs from the geometrical phase between the blades, as observed in the experiments.

Section 3.2 revealed that the global power coefficient evolution with regard to the tip speed ratio of the ducted 2-VATT is unchanged when the flow is misaligned with the turbine heading up to ±15° in the sheared current. We also showed that the average drag coefficient of the turbine increases with the angle of incidence up to +15 % at ±15°. The increase is only of a few percent when $\alpha = \pm 7°$ which indicates that the effect of the misalignment on the drag coefficient is not linear. Some flow detachments from the vertical fairings might occur between 7° and 15°, even though the drag standard deviation is unchanged, that could explain the significant difference between α equals 7° and 15° compared to that between 0° and 7°. In addition, when looking solely at the green rotor column (Fig. 5), in FC, the maximal average power coefficient increases when the column moves upstream and the C_P curves with regard to λ widens when the column moves downstream with a slight decrease of the maximal $\overline{C_P}$. It appeared that the effect of the misalignment on that single column is similar but reversed in the ebb tide configuration, with the increase of maximal average power coefficient when the column moves downstream instead of upstream in FC. That reversed tendency is the same with the 2-VATT fixed on the monopile base so it is rather due to the difference of counter-rotation direction between FC and EC than to the base geometry. Indeed, the blades go against the current along the central fairing in FC whereas that occurs along the lateral fairings in EC. When the flow is misaligned with the turbine heading, we suppose that the local velocity increases on the downstream side of the vertical fairings, similarly to aerofoil extrados. If we

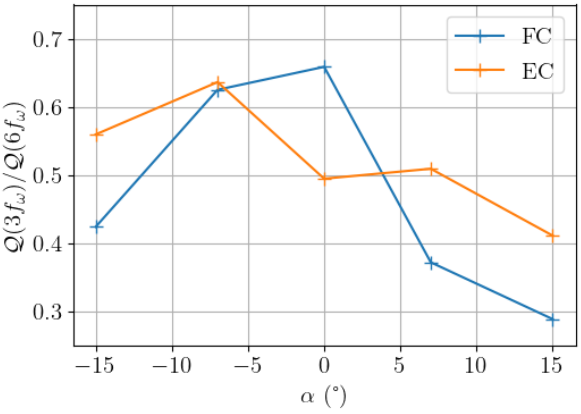

Figure 14: Amplitude ratio between the torque Fourier transform peaks of the the green column at 3 and 6 times the rotational frequency with regard to the flow misalignment angle in EC and FC at the optimal operating point.

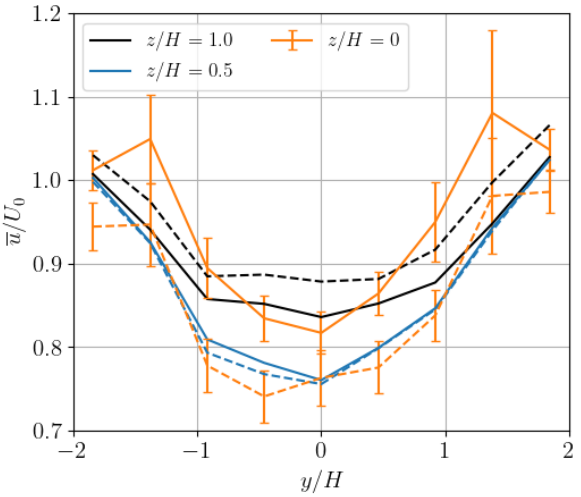

Figure 15: Streamwise velocity horizontal profiles measured by LDV upstream of the turbine at $x/H = -1$ in EC, with the turbine on the tripod base facing a uniform velocity profile (solid lines) and facing a sheared profile (dashed lines). The error bars represent the normalized standard deviation of the streamwise velocity.

still focus on the green rotor column, at $-15°$ for instance, the flow would be accelerated where the blades move in the current direction in the two cases given the rotation direction. Thus, the apparent velocity on the blade would be lowered, which would lower the torque trough and so increase the power coefficient when the column is upstream in FC and downstream in EC.

Furthermore, we observed an increase of $\sigma(C_{Pcol})$ in EC from $\alpha = +15$ to $-15°$, mainly at λ lower than the optimal for the green rotor column but on the whole λ range on the red side, which is also present but less clear on the monopile base, and absent in FC anyway. This result is hardly explained to this date. Similarly, the torque frequency content and its angular distribution evolution with the angle of incidence show that the physical phenomena affecting the ducted 2-VATT behaviour are different between FC and EC. The torque distribution is hardly modified in EC when α increases from -7 to +7° and only the torque magnitude decreases whereas the torque distribution is significantly affected by the flow misalignment in FC. However, the rotor angular position being only relative, we lack the geometrical location of the torque peaks occurrence to explain these phenomena.

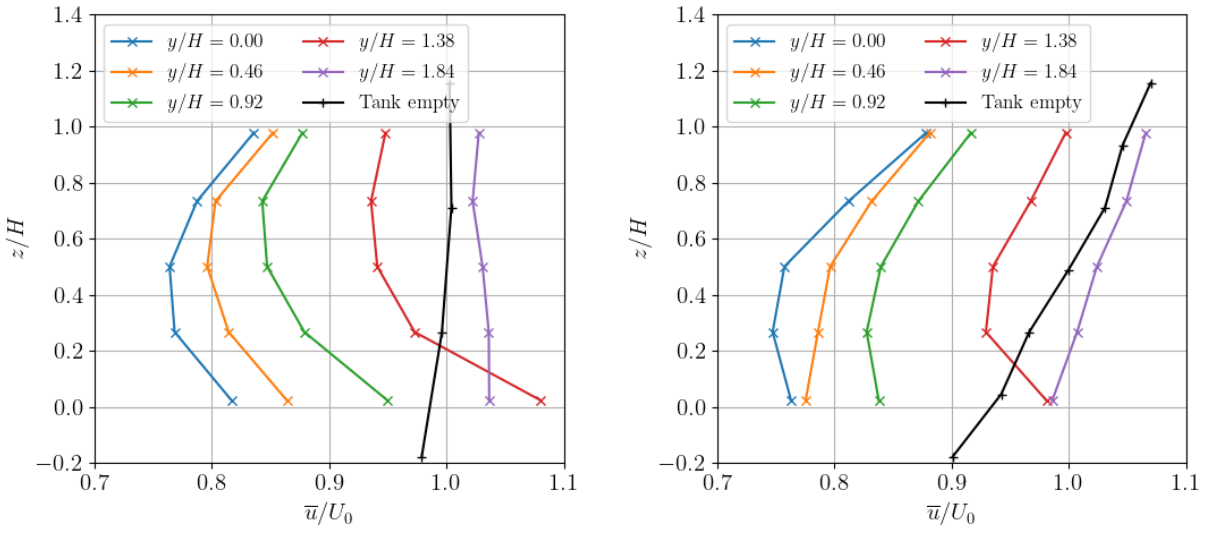

(a) Uniform flow

(b) Sheared flow

Figure 16: Streamwise velocity vertical profiles measured by LDV upstream of the turbine at $x/H = -1$ in EC.

5. Conclusion

Most of the time, tidal turbines tank tests are carried out in idealised current conditions characterised by a uniform velocity over the turbine capture area and a velocity direction collinear with the turbine heading. However, the real tidal currents at sea present vertically sheared velocity profiles and variable directions in space and time. The present study aims at assessing the effect of both the flow shear and its misalignment on the behaviour of a bottom mounted and ducted twin vertical axis tidal turbine (2-VATT). To this end, a 1/20 scale model is tested in Ifremer's wave and current flume tank facing a uniform velocity profile and a sheared one, in ebb and flood tide configurations, with a flow misalignment ranging from -15 to $+15$ degrees.

The results show that the drag and the average power coefficients of the ducted 2-VATT are unaffected by the upstream flow shear. Only the torque angular distributions are modified and so the power coefficient fluctuations are 35 % higher at the optimal operating point in a sheared current compared to a uniform one. The flow misalignment with regard to the turbine heading increases the average drag coefficient by 15 % for a flow incidence of $\pm$ 15°. The power performance of the whole 2-VATT is barely affected by the misalignment as the power lost by one rotor column is roughly compensated by a gain on the other column. However, the misalignment affects the torque angular distribution of a rotor column and does so differently whether the turbine is in the flood or the ebb tide configuration. To explain the physics of these torque distribution changes, we would need better instrumentation such as absolute angular position encoder or separate torque measurements between the upper and the lower rotors. Local flow measurements by particle image velocimetry or numerical simulations would also be of great help to understand the underlying physics. Be that as it may, the increase of torque fluctuations induced by the flow shear and the misalignment must be considered at the design stage of tidal turbines.

6. Acknowledgements

This work was financially supported in part by the French Research and Technology National Association (ANRT) under the convention Cifre n°2020/0688. The authors acknowledge Jean-Valéry Facq and Cédric Derveaux for the design of the turbine model as well as Benoît Gomez and Benoît Gaurier for their help during the experiments.

References

[1] Ahmed, U., Apsley, D.D., Afgan, I., Stallard, T., Stansby, P.K., 2017. Fluctuating loads on a tidal turbine due to velocity shear and turbulence : Comparison of CFD with fi eld data. Renewable Energy 112, 235–246. doi:10.1016/j.renene.2017.05.048.

[2] Cossu, R., Penesis, I., Nader, J.R., Marsh, P., Perez, L., Couzi, C., Grinham, A., Osman, P., 2021. Tidal energy site characterisation in a large tidal channel in Banks Strait, Tasmania, Australia. Renewable Energy 177, 859–870. doi:10.1016/j.renene.2021.05.111.

[3] Draycott, S., Steynor, J., Nambiar, A., Sellar, B., Venugopal, V., 2020. Rotational sampling of waves by tidal turbine blades. Renewable Energy 162, 2197–2209. doi:10.1016/j.renene.2020.10.037.

[4] Druault, P., Gaurier, B., Germain, G., 2022. Spatial integration effect on velocity spectrum: Towards an interpretation of the -11/3 power law observed in the spectra of turbine outputs. Renewable Energy 181, 1062–1080. doi:10.1016/j.renene.2021.09.106.

[5] Filipot, J.F., Prevosto, M., Maisondieu, C., Le Boulluec, M., Thomson, J., 2015. Wave and turbulence measurements at a tidal energy site, in: IEEE/OES 11th Current, Waves and Turbulence Measurement (CWTM), pp. 1–9. doi:10.1109/CWTM.2015.7098128.

[6] Frost, C.H., Evans, P.S., Harrold, M.J., Mason-Jones, A., O'Doherty, T., O'Doherty, D.M., 2017. The impact of axial flow misalignment on a tidal turbine. Renewable Energy 113, 1333–1344. doi:10.1016/j.renene.2017.07.006.

[7] Furgerot, L., Du Bois, P.B., Méar, Y., Morillon, M., Poizot, E., Bennis, A.C., 2018. Velocity profile variability at a tidal-stream energy site (Alderney Race, France): From short (second) to yearly time scales, in: OCEANS and MTS/IEEE Kobe Techno-Oceans, IEEE. pp. 2779–2789. doi:10.1109/OCEANSKOBE.2018.8559326.

[8] Gaurier, B., Germain, G., Facq, J.V., Bacchetti, T., 2018. Wave and current flume tank of IFREMER at Boulogne-sur-mer. Description of the facility and its equipment. Technical Report. IFREMER. doi:10.13155/58163.

[9] Gaurier, B., Ordonez-Sanchez, S., Facq, J.V., Germain, G., Johnstone, C., Martinez, R., Salvatore, F., Santic, I., Davey, T., Old, C., Sellar, B., 2020. MaRINET2 Tidal Energy Round Robin Tests—Performance Comparison of a Horizontal Axis Turbine Subjected to Combined Wave and Current Conditions. Journal of Marine Science and Engineering 8, 463. doi:10.3390/jmse8060463.

[10] Grondeau, M., Guillou, S., Mercier, P., Poizot, E., 2019. Wake of a ducted vertical axis tidal turbine in turbulent flows, LBM actuator-line approach. Energies 12, 4273. doi:10.3390/en12224273.

[11] Guillaud, N., Balarac, G., Goncalvès, E., Zanette, J., 2020. Large eddy simulations on vertical axis hydrokinetic turbines - Power coefficient analysis for various solidities. Renewable Energy 147, 473–486. doi:10.1016/j.renene.2019.08.039.

[12] Harding, S., Bryden, I., 2012. Directionality in prospective Northern UK tidal current energy deployment sites. Renewable Energy 44, 474–477. doi:10.1016/j.renene.2012.02.003.

[13] Jaquier, T., 2011. Hydroliennes à flux transverse : Développement d'un prototype HARVEST en canal. Ph.D. thesis. Université de Grenoble. URL: https://theses.hal.science/tel-01424843.

[14] Jin, G., Zong, Z., Jiang, Y., Zou, L., 2020. Aerodynamic analysis of side-by-side placed twin vertical-axis wind turbines. Ocean Engineering 209, 107296. doi:10.1016/j.oceaneng.2020.107296.

[15] Lewis, M., Neill, S., Robins, P., Hashemi, M., Ward, S., 2017. Characteristics of the velocity profile at tidal-stream energy sites. Renewable Energy 114, 258–272. doi:10.1016/j.renene.2017.03.096.

[16] Lloyd, C., Allmark, M., Ordonez-Sanchez, S., Martinez, R., Johnstone, C., Germain, G., Gaurier, B., Mason-Jones, A., O'Doherty, T., 2021. Validation of the dynamic load characteristics on a Tidal Stream Turbine when subjected to wave and current interaction. Ocean Engineering 222, 108360. doi:10.1016/j.oceaneng.2020.108360.

[17] Magnier, M., Delette, N., Druault, P., Gaurier, B., Germain, G., 2022. Experimental study of the shear flow effect on tidal turbine blade loading variation. Renewable Energy , 100061doi:10.1016/j.renene.2022.05.042.

[18] Martinez, R., Ordonez-Sanchez, S., Allmark, M., Lloyd, C., O'Doherty, T., Germain, G., Gaurier, B., Johnstone, C., 2020. Analysis of the effects of control strategies and wave climates on the loading and performance of a laboratory scale horizontal axis tidal turbine. Ocean Engineering 212, 107713. doi:10.1016/j.oceaneng.2020.107713.

[19] Mendoza, V., Chaudhari, A., Goude, A., 2019. Performance and wake comparison of horizontal and vertical axis wind turbines under varying surface roughness conditions. Wind Energy 22, 458–472. doi:10.1002/we.2299.

[20] Michna, J., Rogowski, K., 2022. Numerical Study of the Effect of the Reynolds Number and the Turbulence Intensity on the Performance of the NACA 0018 Airfoil at the Low Reynolds Number Regime. Processes 10, 1004. doi:10.3390/pr10051004.

[21] Modali, P.K., Vinod, A., Banerjee, A., 2021. Towards a better understanding of yawed turbine wake for efficient wake steering in tidal arrays. Renewable Energy 177, 482–494. doi:10.1016/j.renene.2021.05.152.

[22] Moreau, M., Germain, G., Maurice, G., 2023. Experimental performance and wake study of a ducted twin vertical axis turbine in ebb and flood tide currents at a 1/20th scale. Renewable Energy doi:10.1016/j.renene.2023.05.125.

[23] Moreau, M., Germain, G., Maurice, G., Richard, A., 2022. Sea states influence on the behaviour of a bottom mounted full-scale twin vertical axis tidal turbine. Ocean Engineering 265, 112582. doi:10.1016/j.oceaneng.2022.112582.

[24] Moreau, M., Germain, G., Maurice, G., Richard, A., Coquet, R., 2021. HydroQuest : Feedback from Paimpol-Bréhat and validation of the design method, in: 14th European Wave and Tidal Energy Conference, Plymouth. pp. 2229–1–8.

[25] Ouro, P., Dené, P., Garcia-Novo, P., Stallard, T., Kyozuda, Y., Stansby, P., 2022. Power density capacity of tidal stream turbine arrays with horizontal and vertical axis turbines. Journal of Ocean Engineering and Marine Energy doi:10.1007/s40722-022-00257-8.

[26] Piano, M., Neill, S., Lewis, M., Robins, P., Hashemi, M., Davies, A., Ward, S., Roberts, M., 2017. Tidal stream resource assessment uncertainty due to flow asymmetry and turbine yaw misalignment. Renewable Energy 114, 1363–1375. doi:10.1016/j.renene.2017.05.023.

[27] Shahsavarifard, M., Bibeau, E.L., 2020. Performance characteristics of shrouded horizontal axis hydrokinetic turbines in yawed conditions. Ocean Engineering 197, 106916. doi:10.1016/j.oceaneng.2020.106916.

[28] Shamsoddin, S., Porté-Agel, F., 2016. A Large-Eddy Simulation Study of Vertical Axis Wind Turbine Wakes in the Atmospheric Boundary Layer. Energies 9, 366. doi:10.3390/en9050366.

[29] Slama, M., Pinon, G., El Hadi, C., Togneri, M., Gaurier, B., Germain, G., Facq, J.V., Nuño, J., Mansilla, P., Nicolas, E., Marcille, J., Pacheco, A., 2021. Turbine design dependency to turbulence: An experimental study of three scaled tidal turbines. Ocean Engineering 234, 109035.

doi:10.1016/j.oceaneng.2021.109035.

[30] Vergaerde, A., De Troyer, T., Muggiasca, S., Bayati, I., Belloli, M., Kluczewska-Bordier, J., Parneix, N., Silvert, F., Runacres, M.C., 2020. Experimental characterisation of the wake behind paired vertical-axis wind turbines. Journal of Wind Engineering and Industrial Aerodynamics 206, 104353. doi:10.1016/j.jweia.2020.104353.

[31] Vinod, A., Han, C., Banerjee, A., 2021. Tidal turbine performance and near-wake characteristics in a sheared turbulent inflow. Renewable Energy 175, 840–852. doi:10.1016/j.renene.2021.05.026.